Anal Bioanal Chem (2010) 397:3339–3347
DOI 10.1007/s00216-010-3854-x

ORIGINAL PAPER

Temporal resolution of protein–protein interactions in the live-cell plasma membrane

Julian Weghuber · Stefan Sunzenauer · Birgit Plochberger · Mario Brameshuber · Thomas Haselgrübler · Gerhard J. Schütz

Received: 15 April 2010 / Accepted: 16 May 2010 / Published online: 25 June 2010

Abstract We have recently devised a method to quantify interactions between a membrane protein ("bait") and a fluorophore-labeled protein ("prey") directly in the live-cell plasma membrane (Schwarzenbacher et al. Nature Methods 5:1053–1060 2008). The idea is to seed cells on surfaces containing micro-patterned antibodies against the exoplasmic domain of the bait, and monitor the co-patterning of the fluorescent prey via fluorescence microscopy. Here, we characterized the time course of bait and prey micropattern formation upon seeding the cells onto the micro-biochip. Patterns were formed immediately after contact of the cells with the surface. Cells were able to migrate over the chip surface without affecting the micropattern contrast, which remained constant over hours. On single cells, bait contrast may be subject to fluctuations, indicating that the bait can be released from and recaptured on the micropatterns. We conclude that interaction studies can be performed at any time-point ranging from 5 min to several hours post seeding. Monitoring interactions with time opens up the possibility for new assays, which are briefly sketched in the discussion section.

Keywords Protein–protein interactions · Temporal resolution · Micro-patterned surfaces · Atomic force microscopy · Fluorescence microscopy · Plasma membrane · Lipid rafts

J. Weghuber · S. Sunzenauer · B. Plochberger · M. Brameshuber · T. Haselgrübler · G. J. Schütz (✉)
Biophysics Institute, Johannes Kepler University Linz,
Altenbergerstr.69,
4040 Linz, Austria
e-mail: gerhard.schuetz@jku.at

Introduction

An increasing repertoire of methodologies allows for the analysis of protein–protein interactions, thereby providing an experimental basis for understanding the complex molecular interplay in a cell. It is common practice to determine the local environment of a bait protein by cell lysis, protein extraction and subsequent biochemical analysis of the cluster composition via, e.g., specific labeling, mass spectroscopy or protein microarrays. Such in vitro techniques include standard co-immunoprecipitation [1], but also more advanced techniques like TAP-tag fusion [2]. Bioanalysis after the extraction allows for identification of a priori unknown prey. The critical point, however, is to ensure that the molecular clusters are not affected by the extraction procedure. To circumvent this limitation, researchers attempted to detect protein interaction directly in the cell. One example is the specific staining of the bait environment in the live-cell plasma membrane by prey biotinylation, which can be identified after extraction on antibody microarrays [3]. Further live-cell screening methods include two-hybrid screens [4] or assays based on the complementation of fluorescent proteins [5]. Unfortunately, interactions identified by these approaches can hardly be quantified, thus yielding only a rather vague picture of the real situation in the cell. False positives and negatives further require extensive controls to confirm the hits. Alternative techniques were designed to test for interactions between the bait and a known prey, for example Förster Resonance Energy Transfer (FRET) [6, 7], fluorescence correlation analysis (FCS) [8], proximity ligation [9] or co-immobilization experiments [10]; at the ultimate level, even single molecule co-tracking experiments can be used [11,

12]. Being quantitative to different degrees, these approaches allow for a very detailed analysis of the particular interaction. However, they are difficult to extend to high throughput, and require very careful controls in particular when it comes to detecting weak interactions.

We have previously introduced an assay using micro-patterned surfaces as powerful alternative for detection of protein interactions in vivo [13–16]. The method is characterized by high sensitivity down to the level of single molecules, the capability to detect weak interactions, and high throughput capability, making it applicable as a screening tool. In our proof-of-principle study, we have successfully used the technique for a detailed analysis of the interaction between CD4 and Lck, two proteins involved in early T-cell signaling [17, 18]. Figure 1a illustrates the basic principle. A specific ligand to the exoplasmic domain of the bait is arranged in micropatterns on a glass surface, where the intermediate gaps are passivated with BSA. When cells expressing the bait are plated on such surfaces, the bait follows the antibody patterns. To address bait–prey interactions, the lateral distribution of fluorescently tagged prey is analyzed and compared with the antibody/BSA micropatterns. Interaction leads to pronounced co-patterning, whereas no interaction yields homogeneous prey-distribution.

So far, we have analyzed the interaction properties of two candidate proteins at a certain time-point after seeding the cells on the micro-biochip. Here, we present studies on the kinetics of bait and prey redistribution within the first minutes up to hours after seeding the cells. We found fast rearrangement of bait and prey within minutes after first contact with the surface. Bait–antibody and bait–prey interactions studied in this work were found to be stable within the first hours after seeding, making the quantification within this time-frame reliable. In addition, we characterized the binding and unbinding of the bait in different cell regions, which varies remarkably, depending on the movement of the cell. Finally, we discuss the impact of the binding efficiency of used antibodies on bait redistribution in the plasma membrane.

Results

Characterization of cell morphology and bait redistribution on a micro-biochip

We first used atomic force microscopy (AFM) to get a closer view onto the adhesion process of the cells to the micro-patterned surfaces. A monoclonal anti-GFP capture antibody was assembled in 3-μm micropatterns and T24 cells stably expressing the glycosylphosphatidylinositol-anchored protein (GPI-AP) CD59 [19] fused to GFP were grown on this surface. Figure 1b and d show AFM deflection and topography images of a cell seeded onto the micro-biochip, respectively. The cell efficiently spreads on the surface (enlarged section in Fig. 1c). The flat peripheral regions (0.5 to 1 μm in height) can be nicely discriminated from the central area (up to 6 μm in height) on the topography image. Note that in this case the micropatterns next to the cell give some contrast in the deflection image; we attribute the signal to shedded and crosslinked protein clusters, which are specifically bound to the capture antibody spots via GFP. The residual micro-pattern contrast allows for getting an impression of the adhesion process (see magnification in Fig. 1c): the rim of the lamellipodium correlates with the micropattern structure, indicating that during growth the cell attaches predominantly to the capture antibody sites. Regions away from the cell edge show a rather smooth border and no correlation with the micropattern structure.

Fast rearrangement of bait molecules upon micro-biochip contact

We next analyzed the time needed for redistribution of the bait protein on a micro-biochip. For this, we grew T24 cells stably expressing plasma membrane targeted GPI-DAF-GFP (GPI-anchor of the decay accelerating factor (CD55, [20]) fused to GFP) on a micro-biochip containing an anti-GFP-antibody. During the measurements, the sample was kept in an environmental chamber to maintain appropriate culture conditions. As shown in Fig. 2, the fluorescent bait redistributed on the micro-biochip within the first minutes after seeding the cells (A). By scanning the same area after 30 and 50 min, we could follow the spreading and movement of the cells. After 50 min, the cells were fully attached to the surface. Irrespective of the time of observation, we did not observe any cell regions with homogeneous bait fluorescence, indicating that the redistribution of GPI-DAF-GFP on the anti-GFP-antibody micro-biochip occurred faster than the cell spreading on the surface.

We quantified the micropatterns by assigning a brightness and normalized contrast value to each spot [13], and plotted the data as two-dimensional histograms (B). Contrast values range from ~0.1 to ~0.6, indicating a substantial spot heterogeneity. Consistently, a closer look onto the original data shown in (A) reveals cell regions of varying contrast; in particular, peripheral regions appear at lower contrast. To display the kinetics of micropattern formation we pooled all data, calculated the mean contrast of all spots <C> and plotted it as a function of the time upon seeding the cells onto the chip (C). We found only minute fluctuations, indicating that the average bait rearrangement remains constant over at least 1.5 h.

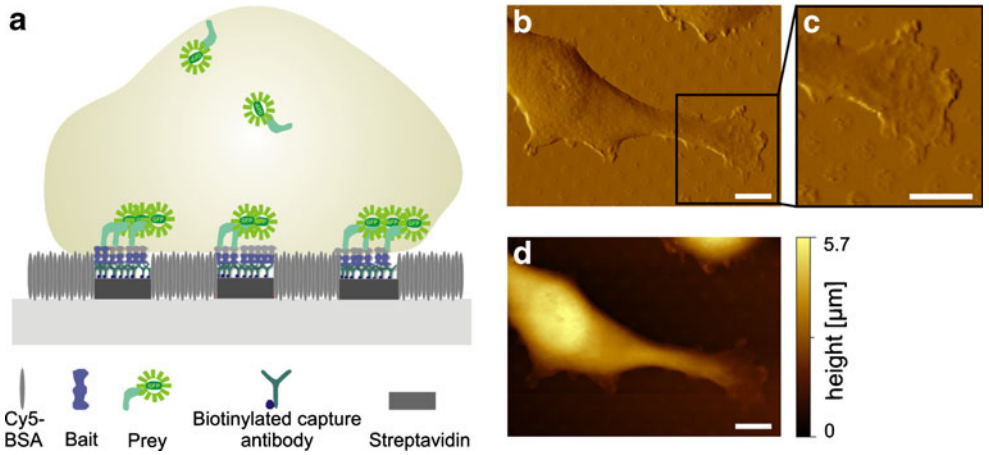

Fig. 1 **a** Schematic illustration of the micropatterning assay. Grids of BSA-Cy5 are printed on functionalized glass coverslips, and interspaces are filled with streptavidin and biotinylated monoclonal antibodies against the membrane protein bait. In cells grown on such micro-biochips, the bait will be arranged in the plasma membrane according to the antibody micropattern. Interactions with a second fluorescently-labeled protein (*prey*) are probed by measuring the degree of co-patterning (reprinted from [13]). **b**–**d** Atomic force microscopy of a T24 cell expressing CD59-GFP and grown on an anti-GFP-antibody coated micro-biochip. **b** and **d** show the deflection and topography image, respectively. **c** is a magnification of the lamellipodium visible in **b**. Note the residual micropattern contrast observable in the deflection images, which allow for correlating the cell morphology with the spots containing capture antibody. *Scale bars* 10 µm

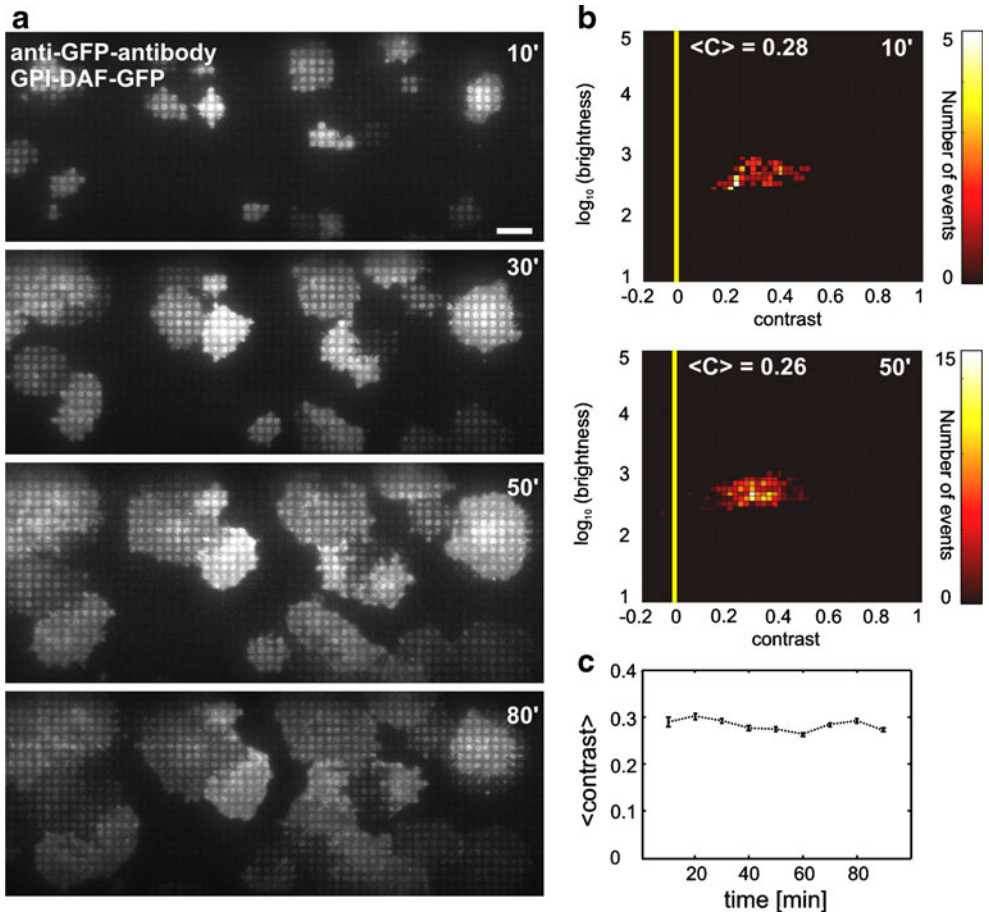

Fig. 2 Bait redistribution using anti-GFP-antibody-coated micro-biochips. **a** T24 cells expressing GPI-DAF-GFP were seeded on a micro-biochip coated with anti-GFP-antibody and scanned 10, 30, 50, and 80 min after seeding. *Scale bars* 20 µm. Statistical analysis of all cells in the scanning area (after 10 and 50 min) is shown in color density plots for the fluorescence brightness F and mean contrast <C> (**b**). **c** Mean contrast <C> of GPI-DAF-GFP versus time after seeding the cells

Temporal resolution of fluorescence intensity variations within single cells

To investigate the binding and unbinding properties of the bait protein to the capture antibody, we analyzed the intensity fluctuations of individual fluorescent spots located at different regions of a single cell. As sample we used again T24 cells expressing GPI-DAF-GFP and a micro-biochip containing anti-GFP-antibody. After seeding the cells, data were recorded in 10 min intervals up to 90 min (Fig. 3a and b). While the intensity of spots in central regions of the cell remained constant (e.g., spot marked with a blue circle), we detected considerable fluctuations of the spot intensities in some peripheral regions (e.g., spot marked with red circle). The observed intensity variations resulted from the spreading and retraction of the cell, which was especially pronounced for the analyzed cell between 60 and 90 min. Comparison of the upper left area after 70, 80, and 90 min shows retraction and re-growth of the cell (e.g., green and yellow circle) within this time-span. Thus, the interaction of bait and surface-antibody is lost and can be re-established in the same region of the micro-biochip during movement of the cell.

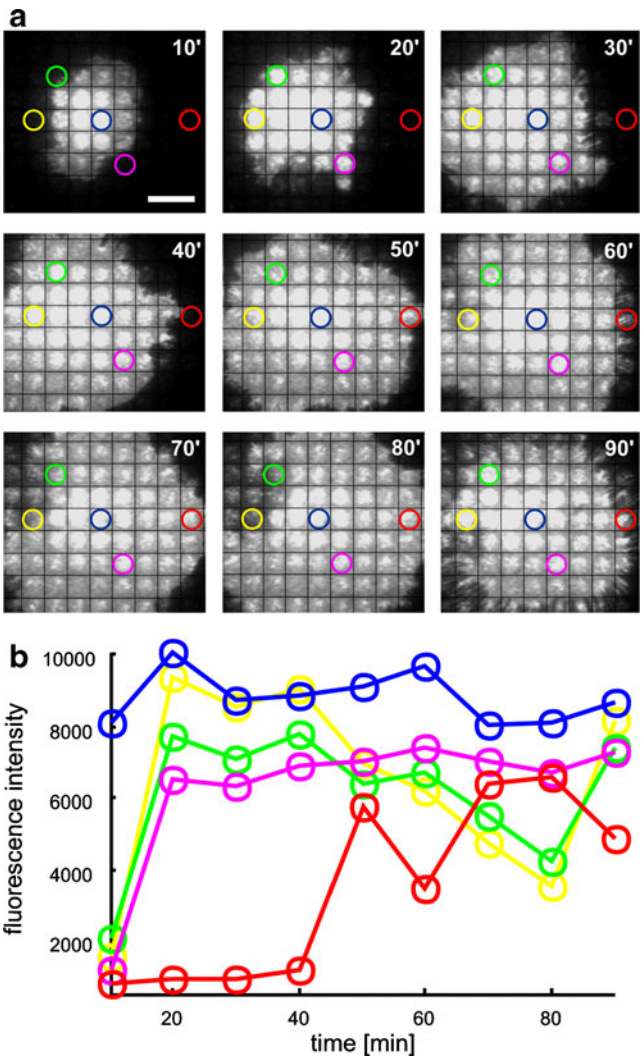

Fig. 3 Fluorescence intensity variations within single cells. **a** T24 cells expressing GPI-DAF-GFP were grown on a micro-biochip coated with anti-GFP-antibody. A single cell was scanned in 10-min intervals up to 90 min after seeding. *Scale bar* 10 µm. **b** Analysis of the fluorescence intensity of single spots within the cell at indicated time points. *Colors* of the plot represent the position of the observed spot marked with the respective circle in (**a**)

Viability of cells grown on micro-biochips

In order to check the suitability of our experimental setup to monitor protein–protein interactions for longer time periods we grew cells stably expressing the GPI-anchored protein CD59-GFP on an anti-CD59-antibody micro-biochip, and repeatedly scanned the same area. The images in Fig. 4a show the same region after 0.5, 2.5, 3.5, and 4.5 h. Importantly, after attachment, the cells undergo morphological transitions and are still mobile after 4.5 h. Based on these results, we conclude that the cell viability is maintained and long-time measurements can be performed under the described experimental conditions. Bait micropatterns remained similar in contrast during the excursions of the cells on the surface (Fig. 4a right column, and Fig. 5 red circles), thus providing a stable capture matrix for the prey.

Monitoring direct and indirect protein–protein interactions over hours

In addition to the bait redistribution we also analyzed the behavior of the prey GPI-DAF-GFP on an anti-CD59-antibody micro-biochip. GPI-anchored proteins have been reported to partition into lipid rafts, nanometer-sized lipid domains in the plasma membrane [21–23]. Currently, a few methods allow for analysis of protein co-recruitment to lipid rafts in biomembranes [24–27], yet there is no methodology that allows for measurements in a live-cell context. We thus asked whether our micropatterning approach enables the detection of the indirect interaction between two GPI-APs, using CD59 as bait. To restrict the analysis to indirect interactions mediated by the lipid environment we used as prey GPI-DAF-GFP, which consists essentially of a lipid-anchored GFP without additional protein interaction motifs. Indeed, the fluorescent prey has redistributed on the anti-CD59-antibody micro-biochip (Fig. 4b). We next scanned the same population of cells after 2.5, 3.5, and 4.5 h and found prey micropatterns of similar contrast at all time points. The mean contrast <C> on the anti-CD59-antibody biochip was stable over time for both CD59-GFP and GPI-DAF-GFP (Fig. 5). The mean contrast obtained for CD59-GFP (0.08 to 0.14) was slightly higher than for GPI-DAF-GFP (0.04 to 0.08),

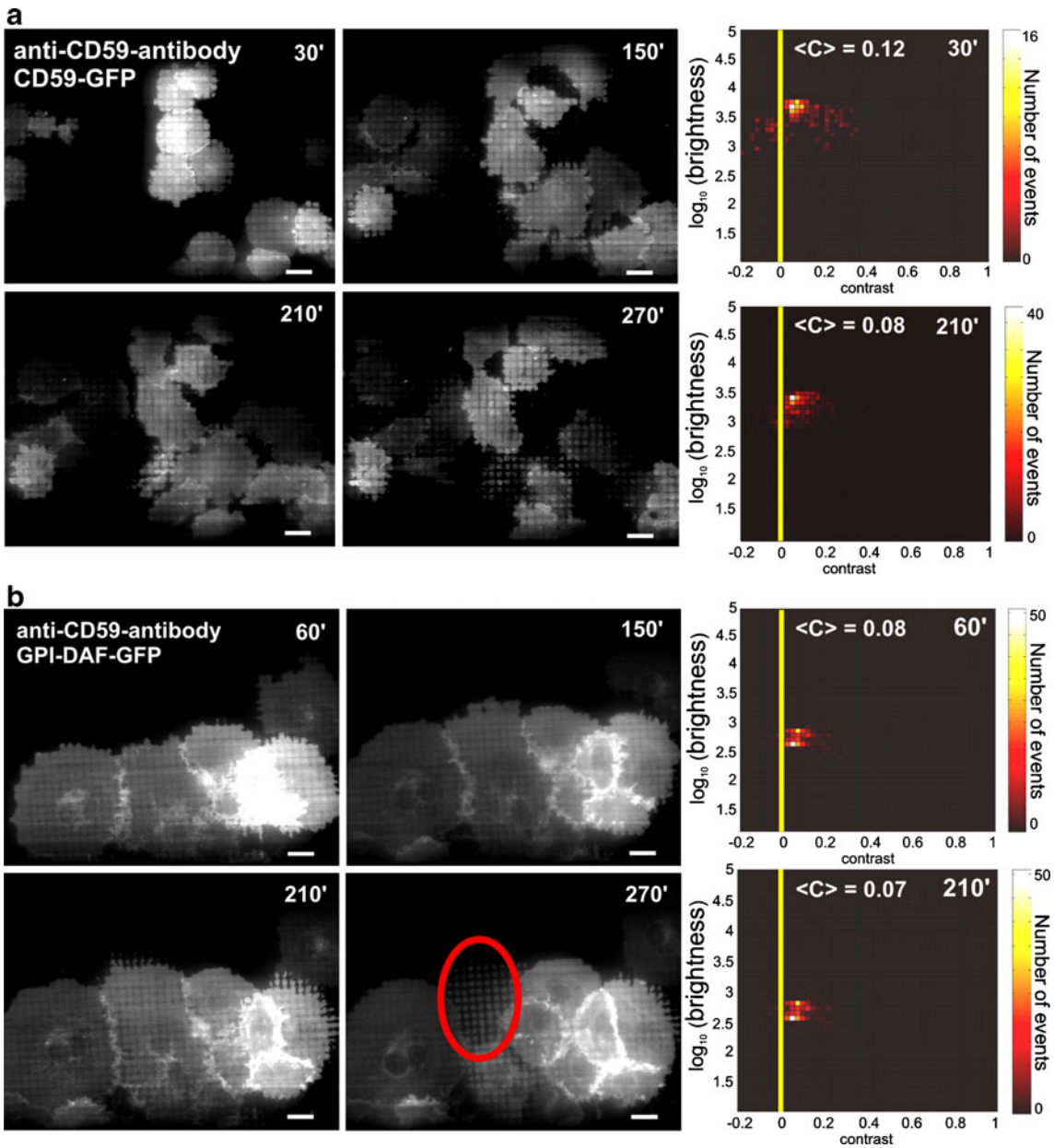

Fig. 4 Bait and prey redistribution on micro-biochips coated with anti-CD59-antibody. T24 cells expressing CD59-GFP (**a**) or GPI-DAF-GFP (**b**) were seeded on micro-biochips coated with anti-CD59-antibody and scanned 30 (60), 150, 210, and 270 min after cell seeding. Statistical analysis of all cells in the scanning area is shown for exemplary time points in the color density plot (*right column*). The *red circle* (**b**, 270 min) indicates a region of high contrast detected after detachment of a cell in this region. *Scale bars* 20 µm

which is a consequence of the direct interaction of CD59-GFP with the capture antibody.

Note that occasionally cells were found to undergo cell death during the measurement time (e.g., the cell marked with a red circle in Fig. 4b), which was accompanied by the retraction of the extended lamellipodia. In such cases, a considerable quantity of fluorescent prey remained on the surface, leading to high contrast values in these areas. Consistently, laser scanning confocal microscopy of such regions revealed fluorescent prey only in z-sections next to the micro-biochip surface (red circled region in Fig. 6). Distinct from that, intact cells were characterized by homogeneous fluorescence and the presence of fluorescent prey throughout the cell when choosing the same scanning height (note that confocal microscopy has a too large depth of focus to detect micropatterns in case of weak bait–prey interactions). It is thus important for appropriate analysis to ensure that the observed prey micropatterns indeed correspond to a living cell, for example by monitoring a transmission light image in parallel. Alternatively, one may identify appropriate time frames, in which cell retraction hardly happens. For the investigated interaction

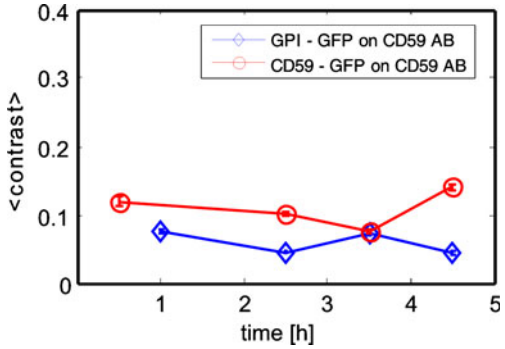

Fig. 5 Mean contrast of bait and prey redistribution over time. Comparison of the mean contrast of CD59-GFP and GPI-DAF-GFP on a micro-biochip coated with anti-CD59-antibody at the time points shown in Fig. 4 (30/60, 150, 210 and 270 min after seeding). *Error bars* indicate standard error of the mean

of GPI-DAF-GFP and CD59 it has turned out that measurements within the first three hours are hardly affected by such retractions.

Antibody binding properties influence bait redistribution

Comparison of Figs. 2 and 4 indicates different bait contrast when using the anti-GFP-antibody compared to anti-CD59-antibody. While cells grown on anti-CD59-antibody micro-biochips were characterized by the same contrast all over the plasma membrane, contrast values varied significantly when the anti-GFP-antibody was used: cells displayed regions with high contrast in the central regions of the cells, but low contrast in peripheral cell areas. We interpret these findings as a consequence of the binding kinetics of the used antibodies (Fig. 7). In general, synthesized or recycled proteins will be transported predominantly to central regions of the cellular plasma membrane, with less transport pathways ending in lamellipodia. If the binding efficiency of the used antibody is high, the predominant fraction of GPI-APs will be immobilized by the capture antibody directly at the fusion sites of the transport vesicles (cartoon in Fig. 7a), yielding concurrently a reduced bait density and contrast in the periphery. Contrary, if the binding efficiency is low, the majority of the bait will diffuse over substantial portions of the cell surface before being immobilized, which results in a homogenous but lower contrast all over the plasma membrane (cartoon in Fig. 7b).

To test this model, we targeted the same bait protein (CD59-GFP) by two antibodies with different binding efficiency (anti-GFP or anti-CD59). Indeed, we found cell regions with high and with low contrast values when using the anti-GFP-antibody (high binding efficiency), while contrast was identical all over the cell membrane when the anti-CD59-antibody (low binding efficiency) was used (see images in Fig. 7a and b). In consequence, statistical analysis will result in a broad contrast range if the binding efficiency of the antibody is high, but a narrow one if the binding efficiency is low.

Discussion

The micropatterning technique appears intriguingly simple for analysis of protein interaction in live cells. Yet, in order to correctly interpret the resulting images temporal resolution is helpful. In this report, we provide first insights into the kinetics of the formation of bait and prey micropatterns.

Firstly, the interaction properties between bait and prey can be analyzed from 5 min after seeding the cells to the micro-biochip, and may be continued for hours as long as the culture conditions are adequate. Here, we show that the interaction properties of the analyzed proteins may be calculated within the first 4 h after plating, since the contrast levels remained constant within this time-frame. On the single cell level, however, the brightness and thus the bait content of individual spots may well vary with time, indicating that bait can be released from and recaptured on the micropatterns, as the cells are moving over the surface.

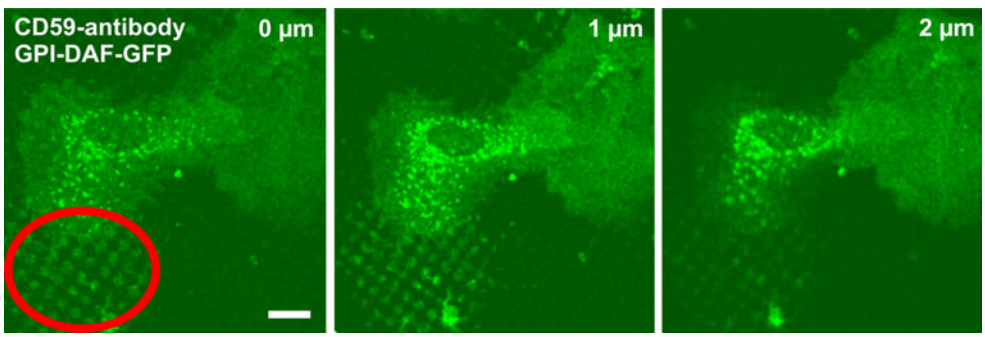

Fig. 6 High contrast regions detected after cell detachment. T24 cells expressing GPI-DAF-GFP were grown for 12 h on a micro-biochip coated with anti-CD59-antibody and fixed. Laser scanning confocal microscopy was used to analyze regions of high contrast resulting from cell detachment. Images were collected at 1 µm intervals to create a stack in *Z* axis. The *red circle* indicates a region from which the cell has retracted; no additional fluorescence is observable from sections above this region. *Scale bars* 10 µm

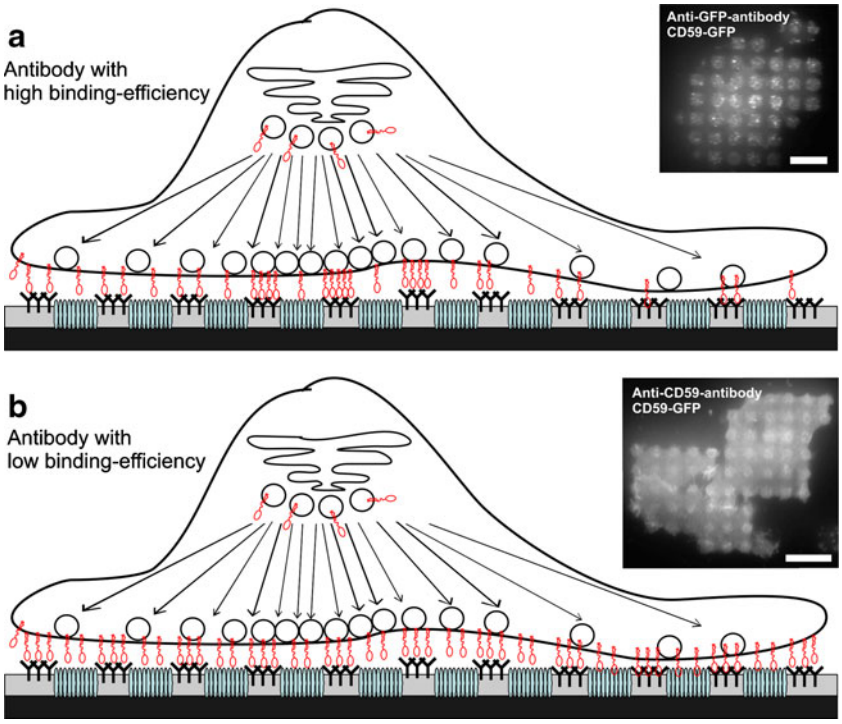

Fig. 7 Effects of the antibody binding efficiency on the redistribution of GPI-APs. A high binding efficiency of the capture antibody results in immobilization of the bait immediately upon delivery to the plasma membrane, thus yielding high contrast near the sites of vesicle fusion, but low contrast at peripheral regions (**a**). Weak binding affinity allows the bait to diffuse over the plasma membrane, resulting in intermediate contrast levels all over the cell surface (**b**). The insets show T24 cells expressing CD59-GFP on a micro-biochip coated with the high affinity antibody anti-GFP (**a**) or the low-affinity antibody anti-CD59 (**b**). *Scale bars* 10 μm (**a**) or 15 μm (**b**)

Secondly, we occasionally observed that retracting cells (e.g., cells undergoing cell death) may leave fluorescent bait or prey during their movement. Control over the cell shape in particular in peripheral regions thus is important to avoid misinterpretations. Note that we observed such traces of prey only in case of proteins that showed bait interaction; therefore misinterpretation appears to affect only quantitative analysis.

Thirdly, the obtained bait contrast depends on the affinity of the used capture antibodies. Weak affinity antibodies have the particular advantage that the same bait contrast can be generated all over the cell surface, which allows for straightforward image analysis and improved comparability of data sets obtained on different cells.

We foresee particular applications for the time-resolved analysis, which are summarized in Fig. 8. The analysis of protein interactions in migrating cells (Fig. 8a) is of great interest in order to detect leading-edge specific interactions in polarized cells [28]. Potential target molecules include integrins [29], actin-regulating proteins [30] or regulators of cell polarity like CdC42 [31] or PAK1 [32]. To stimulate the synchronized migration of the target cells expressing bait and prey, the establishment of a chemokine concentration gradient in the subphase above the micro-biochip seems feasible. Another suitable application would be the analysis of cell-cycle-dependent protein interactions (Fig. 8b): a stimulus may lead to strong interaction of two candidate proteins in S-phase, weak interaction in G2-phase and finally no interaction after mitosis. Exemplarily, the stimulus could be the expression of a cyclin-dependent kinase, leading to polarized growth and thus varying interactions of proteins during the cell cycle, which are needed for the necessary morphological transitions [33]. These interactions can be continuously evaluated on the micro-biochip. Finally, spatial and temporal resolution of large protein clusters becomes possible (Fig. 8c). For instance, protein interactions could be analyzed during the formation of the immunological synapse, the interface between an antigen-presenting cell and a lymphocyte [34, 35].

Material and methods

DNA constructs and reagents

The pCR3 GPI-DAF-GFP, a GFP modified by the GPI-anchor of decay accelerating factor (CD55/DAF) [36] was kindly provided by Daniel Legler (University of Konstanz, Switzerland), the CD59-GFP was a kind gift by Jennifer Lippincott-Schwartz (NIH, Bethesda, USA). The monoclonal antibodies against CD59 (epitope MEM-43) and GFP were purchased from Antibodies online, Herford, Germany.

Cell culture

Media, fetal bovine serum (FBS), antibiotics and Geneticin (G418 sulfate) were purchased from PAA Laboratories GmbH, Pasching, Austria; Culture plates were from Greiner Bio One International, Austria. Human T24 cells were from

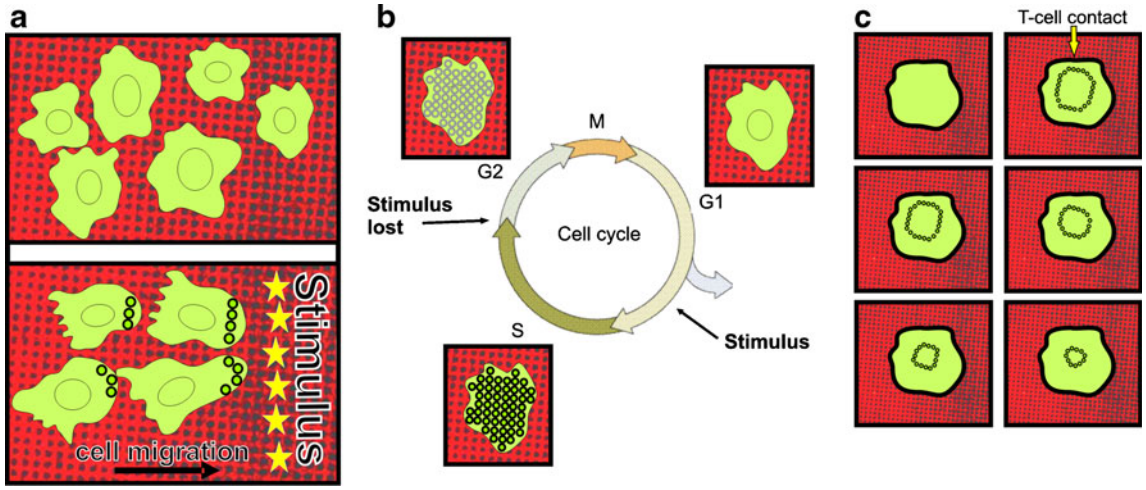

Fig. 8 Potential applications of time-resolved protein–protein interaction analysis in live cells. **a** Analysis in migrating cells. A stimulus initiates cell polarization and leading-edge specific interaction of bait and prey. **b** Determination of cell-cycle-dependent protein–protein interactions. In this example, bait and prey do not interact with each other in G1-phase. A stimulus leads to strong interaction in S-phase and, after the stimulus is lost, weak interaction in G2-phase. **c** Spatial and temporal resolution of protein interactions within the developing immunological synapse (IS). Large-scale protein segregation within the synapse may modulate the interaction patterns in a spatiotemporal way, thereby regulating downstream signaling

American Type Culture Collection; a Gene Pulser electroporation unit (X-cell) and electroporation cuvettes were from Bio-Rad, CA, USA.

T24 cells were cultured in RPMI medium supplemented with 10% FBS and grown at 37°C in a humidified incubator (≥95%) with 5% CO_2. 70% confluent cells were harvested and transfected with 10 µg plasmid DNA using the X-Cell electroporator with following electroporation conditions: 240 V, 950 µF, unlimited resistance, 4-mm gap cuvettes and RPMI16 without FBS as the electroporation-buffer. Cells were plated into 100-mm culture dishes and grown for 48 h. The medium was removed and replaced with fresh medium supplemented with 400 µg/ml G418. Medium was changed every 3 days, and 15–20 days later individual neomycin-resistant colonies were selected for propagation and analysis.

For AFM studies, cells were plated on micro-biochips and left for the indicated times, and subsequently fixed in 4% paraformaldehyde (Sigma Aldrich, Germany) for 10 min at 37°C.

Microcontact printing, microscopy, and data analysis

µ-Contact printing and microscopy were performed as previously reported [13]. Micro-biochips were scanned in a humidified heating stage set at 37°C with 5% CO_2 regulated by an external controller (Pecon, Erbach, Germany). In addition, an objective heater (Chromophor Technologies, Fuessen, Germany) was used to keep the temperature of the TIRF objective at 37°C. During microscopy, cells were kept in the same RPMI growth medium including FBS, as used for culturing.

Data analysis was performed as described [13]. Briefly, the BSA-Cy5 image was used for an automatic gridding algorithm to determine the rotation of the image with respect to the scan direction characterized by the angle ϕ, and the grid-size. Based on the grid, images were segmented into squares containing both the BSA-Cy5 and capture mAb regions. A circle with a diameter of 4 µm was projected into the center: each square was characterized by the mean fluorescence intensity within the circle, F^+, and the remaining part of the square, F^-. In addition, the background signal of the glass surface was determined on a part of the chip containing no cells (F_{bg}). For analysis of multiple cells, we plotted two-dimensional histograms of the fluorescence signal $F = F^+ - F_{bg}$ on the ordinate against the signal contrast $C = \frac{F^+ - F^-}{F^+ - F_{bg}}$ on the abscissa. To restrict the analysis to cells expressing fluorescent proteins, only squares with a signal exceeding a preset threshold value were used for analysis.

Laser scanning confocal microscopy

LSM images were taken with a LSM 510 Meta confocal laser scanning microscope using a 40× 1.2 NA water immersion objective (Zeiss).

Atomic force microscopy

A PicoPlus AFM (Molecular Imaging, Tempe, USA) was placed on an Axiovert 200 inverted optical microscope (Zeiss GmbH, Oberkochen, Germany) via a quickslide stage (Molecular Imaging, Tempe, USA). The sample was mounted on a high-precision XY-stage (Scan IM 120 × 100,

Märzhäuser, Germany). This stage allows for convenient changing and positioning of samples, as the sample holder can be moved both relative to the optical axis of the objective, and also relative to the AFM cantilever. The whole setup was placed on a passive antivibration optical table (Newport GmbH, Darmstadt, Germany) without any additional damping system. For AFM imaging, the scanner was used in contact mode (10 pN/nm silicon nitride cantilevers).

Acknowledgments This work was supported by the Austrian Science Fund (project Y250-B3), the European Science Foundation (LIPIDPROD, # I301-B12), the EU FP7-project "Single Molecule Workstation" (Project no.: 213717), the Austrian Academy of Science DOC-fForte stipendium and the GEN-AU project of the Austrian Research Promotion Agency. We thank J. Lippincott-Schwartz (US-NIH) and D. Legler (University of Konstanz) for providing plasmids.

References

1. Barrios-Rodiles M, Brown KR, Ozdamar B, Bose R, Liu Z, Donovan RS, Shinjo F, Liu Y, Dembowy J, Taylor IW, Luga V, Przulj N, Robinson M, Suzuki H, Hayashizaki Y, Jurisica I, Wrana JL (2005) Science 307:1621–1625
2. Puig O, Caspary F, Rigaut G, Rutz B, Bouveret E, Bragado-Nilsson E, Wilm M, Seraphin B (2001) Methods 24:218–229
3. Kotani N, Gu J, Isaji T, Udaka K, Taniguchi N, Honke K (2008) Proc Natl Acad Sci USA 105:7405–7409
4. Uetz P, Giot L, Cagney G, Mansfield TA, Judson RS, Knight JR, Lockshon D, Narayan V, Srinivasan M, Pochart P, Qureshi-Emili A, Li Y, Godwin B, Conover D, Kalbfleisch T, Vijayadamodar G, Yang M, Johnston M, Fields S, Rothberg JM (2000) Nature 403:623–627
5. Hu CD, Chinenov Y, Kerppola TK (2002) Mol Cell 9:789–798
6. Jares-Erijman EA, Jovin TM (2003) Nat Biotechnol 21:1387–1395
7. Maurel D, Comps-Agrar L, Brock C, Rives ML, Bourrier E, Ayoub MA, Bazin H, Tinel N, Durroux T, Prezeau L, Trinquet E, Pin JP (2008) Nat Methods 5:561–567
8. Schwille P, Meyer-Almes FJ, Rigler R (1997) Biophys J 72:1878–1886
9. Soderberg O, Gullberg M, Jarvius M, Ridderstrale K, Leuchowius KJ, Jarvius J, Wester K, Hydbring P, Bahram F, Larsson LG, Landegren U (2006) Nat Methods 3:995–1000
10. Dorsch S, Klotz KN, Engelhardt S, Lohse MJ, Bunemann M (2009) Nat Methods 6:225–230
11. Dunne PD, Fernandes RA, McColl J, Yoon JW, James JR, Davis SJ, Klenerman D (2009) Biophys J 97:L5–L7
12. Ruprecht V, Brameshuber M, Schutz GJ (2010) Soft Matter 6:568–581
13. Schwarzenbacher M, Kaltenbrunner M, Brameshuber M, Hesch C, Paster W, Weghuber J, Heise B, Sonnleitner A, Stockinger H, Schutz GJ (2008) Nat Methods 5:1053–1060
14. Weghuber J, Brameshuber M, Sunzenauer S, Lehner M, Paar C, Haselgrübler T, Schwarzenbacher M, Kaltenbrunner M, Hesch C, Paster W, Heise B, Sonnleitner A, Stockinger H, Schutz GJ (2010) Detection of protein–protein interactions in the live cell plasma membrane by quantifying prey redistribution upon bait micro-patterning. Methods Enzymol 472:133–151
15. Brameshuber M, Schwarzenbacher M, Kaltenbrunner M, Hesch C, Paster W, Weghuber J, Heise B, Sonnleitner A, Stockinger H, Schutz GJ (2009) Nature Methods 6:183–184
16. Weghuber J, Sunzenauer S, Brameshuber M, Plochberger B, Hesch C, Schutz GJ (2010) J Vis Exp Mar 19 (37)
17. Turner JM, Brodsky MH, Irving BA, Levin SD, Perlmutter RM, Littman DR (1990) Cell 60:755–765
18. Shaw AS, Chalupny J, Whitney JA, Hammond C, Amrein KE, Kavathas P, Sefton BM, Rose JK (1990) Mol Cell Biol 10:1853–1862
19. Walsh LA, Tone M, Thiru S, Waldmann H (1992) Tissue Antigens 40:213–220
20. Mikesch JH, Buerger H, Simon R, Brandt B (2006) Biochim Biophys Acta 1766:42–52
21. Pike LJ (2006) J Lipid Res 47:1597–1598
22. Sprenger RR, Speijer D, Back JW, De Koster CG, Pannekoek H, Horrevoets AJ (2004) Electrophoresis 25:156–172
23. MacLellan DL, Steen H, Adam RM, Garlick M, Zurakowski D, Gygi SP, Freeman MR, Solomon KR (2005) Proteomics 5:4733–4742
24. Baumgart T, Hammond AT, Sengupta P, Hess ST, Holowka DA, Baird BA, Webb WW (2007) Proc Natl Acad Sci USA 104:3165–3170
25. Lingwood D, Ries J, Schwille P, Simons K (2008) Proc Natl Acad Sci USA 105:10005–10010
26. Kaiser HJ, Lingwood D, Levental I, Sampaio JL, Kalvodova L, Rajendran L, Simons K (2009) Proc Natl Acad Sci USA 106:16645–16650
27. Sengupta P, Hammond A, Holowka D, Baird B (2008) Biochim Biophys Acta 1778:20–32
28. Vicente-Manzanares M, Webb DJ, Horwitz AR (2005) J Cell Sci 118:4917–4919
29. Vicente-Manzanares M, Choi CK, Horwitz AR (2009) J Cell Sci 122:199–206
30. Le CC, Carlier MF (2008) Physiol Rev 88:489–513
31. Itoh RE, Kurokawa K, Ohba Y, Yoshizaki H, Mochizuki N, Matsuda M (2002) Mol Cell Biol 22:6582–6591
32. Li Z, Hannigan M, Mo Z, Liu B, Lu W, Wu Y, Smrcka AV, Wu G, Li L, Liu M, Huang CK, Wu D (2003) Cell 114:215–227
33. Moseley JB, Nurse P (2009) Curr Opin Cell Biol 21:82–88
34. Dustin ML (2008) Adv Exp Med Biol 640:164–182
35. Dustin ML (2007) Curr Opin Cell Biol 19:529–533
36. Legler DF, Doucey MA, Schneider P, Chapatte L, Bender FC, Bron C (2005) FASEB J 19:73–75